PERGAMON

International Journal of Heat and Mass Transfer 45 (2002) 1477–1492

International Journal of HEAT and MASS TRANSFER

www.elsevier.com/locate/ijhmt

MHD free convection in a liquid-metal filled cubic enclosure. I. Differential heating

Ivan Di Piazza [1], Michele Ciofalo *

Dipartimento di Ingegneria Nucleare, Università di Palermo, Viale delle Scienze, I-90128 Palermo, Italy

Received 24 July 2000; received in revised form 6 July 2001

Abstract

The buoyancy-driven magnetohydrodynamic flow in a liquid-metal filled cubic enclosure was investigated by three-dimensional numerical simulation. The enclosure was differentially heated at two opposite vertical walls, all other walls being adiabatic, and a uniform magnetic field was applied orthogonal to the temperature gradient and to the gravity vector. The Rayleigh number was 10^5 and the Prandtl number was 0.0321 (characteristic of Pb–17Li at 573 K). The Hartmann number was made to vary between 10^2 and 10^3 and the electrical conductance of the walls between 0 and ∞. The continuity, momentum and enthalpy transport equations, in conjunction with a Poisson equation for the electric potential, were solved by a finite volume method using the general-purpose CFX-4 package with some necessary adaptations. Steady-state conditions were assumed. With respect to the case of parallel flow in an infinitely tall enclosure, studied in previous work, the suppression of convective motions due to magnetohydrodynamic interactions was stronger in the core, and a complex three-dimensional flow (with secondary motions) and current pattern was established in the fluid domain. Increasing the Hartmann number suppressed convective motions and exalted the square-shape of the circulation cells. Increasing the wall conductance ratio from perfectly insulating to perfectly conducting walls also resulted in an increasing suppression of convection. The related case of an *internally heated* enclosure is discussed in a companion paper. © 2002 Published by Elsevier Science Ltd.

1. Introduction

Different schemes have been proposed in the last years for the breeding blankets of fusion reactors; some of them are based on solid breeders such as lithium hydrides or silicates, while others rely on liquid lithium alloys, among which the 17%Li–83%Pb eutectic (Pb–17Li) is the most likely candidate. In their turn, liquid metal breeder designs can be classified into two families: in one of them the coolant coincides with the liquid breeder itself (self-cooled concept), while in the other heat is removed by water flowing in tubes (water-cooled concept).

Comparisons of the two concepts have been presented for some considerable time in the context of European projects [1]. In the self-cooled concept high velocities are required to remove heat; thus, the flow must be strongly forced, which results in large pressure losses induced by MHD effects, while buoyancy effects are comparatively negligible. This is not the case for separately-cooled designs, where a weak forced flow is required only for tritium extraction, and relevant temperature gradients occur; therefore, the flow is mainly buoyancy-driven.

Within the separated-cooled concept, the problem arises of understanding and characterizing buoyant flows in a low-Prandtl number fluid under the influence of a strong magnetic field.

In a previous paper [2], a general computational approach to MHD problems using an advanced CFD package with a minimum of modifications was described. The method was validated against asymptotic results for the case of fully developed buoyant flow. The use of a general-purpose package in MHD modelling

* Corresponding author. Tel.: +39-091-232-257/228; fax: +39-091-232-215.

E-mail address: ciofalo@din.din.unipa.it (M. Ciofalo).

[1] Present address: CRS4, VI Strada Ovest, Z.I. Macchiareddu, I-09010 Uta (Cagliari), Italy.

0017-9310/02/$ - see front matter © 2002 Published by Elsevier Science Ltd.
PII: S0017-9310(01)00252-6

Nomenclature

$\mathbf{B}(B)$	magnetic induction vector (module) (T)
c_w	wall conductance ratio, $(\sigma_w t_w)/(\sigma D)$ (dimensionless)
D	side length of the enclosure (m)
$\mathbf{g}(g)$	gravity acceleration vector (module) (m s^{-2})
$\mathbf{j}(j)$	current density vector (module) normalized by $j_0 = \sigma u_0 B$ (dimensionless)
M	Hartmann number, $DB(\sigma/\mu)^{1/2}$ (dimensionless)
Nu	Nusselt number, $(q''D)/(\lambda\Delta\vartheta)$ (dimensionless)
p	pressure normalized by Dj_0B (dimensionless)
Pr	Prandtl number, ν/α (dimensionless)
q''	heat flux (W m^{-2})
Ra	Rayleigh number, $g\beta\Delta\vartheta D^3/(\nu\alpha)$ (dimensionless)
Re_m	magnetic Reynolds number, $u_0 D\sigma\eta$ (dimensionless)
t_w	wall thickness (m)
T	dimensionless temperature, $(\vartheta - \langle\vartheta\rangle)/\Delta\vartheta$ (dimensionless)
u_0	velocity scale, $(\alpha/D)(Ra/M^2)$ (m s^{-1})
$\mathbf{v}(u,v,w)$	velocity vector (components) normalized by u_0 (dimensionless)
x,y,z	co-ordinates normalized by D (dimensionless)

Greek symbols

α	thermal diffusivity (m^2 s^{-1})
β	thermal expansion coefficient (K^{-1})
δ_H, δ_S	thickness of the Hartmann and side layers normalized by D (dimensionless)
$\Delta\vartheta$	wall-to-wall temperature drop (K)
η	magnetic permeability (Ω s m^{-1})
ϑ	temperature (K)
φ	electrical potential normalized by Du_0B (dimensionless)
λ	thermal conductivity (W m^{-1} K^{-1})
μ	viscosity (N s m^{-2})
ν	kinematic viscosity (m^2 s^{-1})
ρ	density (kg m^{-3})
σ	electrical conductivity ((Ω m)$^{-1}$)

Subscripts

H	Hartmann layer
S	side layer
w	wall

opens the possibility of performing numerical simulations for complex geometries of direct engineering interest.

In the present work, the method is applied to the case of a fully three-dimensional buoyancy-induced flow under the influence of a strong magnetic field. The configuration studied (cubic enclosure of side length D with gravity vector, magnetic field, and temperature gradient orthogonal to one another and to the walls) is sketched in Fig. 1(a). The temperature gradient is supposed to be directed along x and the magnetic field along y.

Here, in contrast with the previous fully developed flow problem, convective terms are important and a fully three-dimensional flow occurs; no exact solution exists so that the computational results can only be

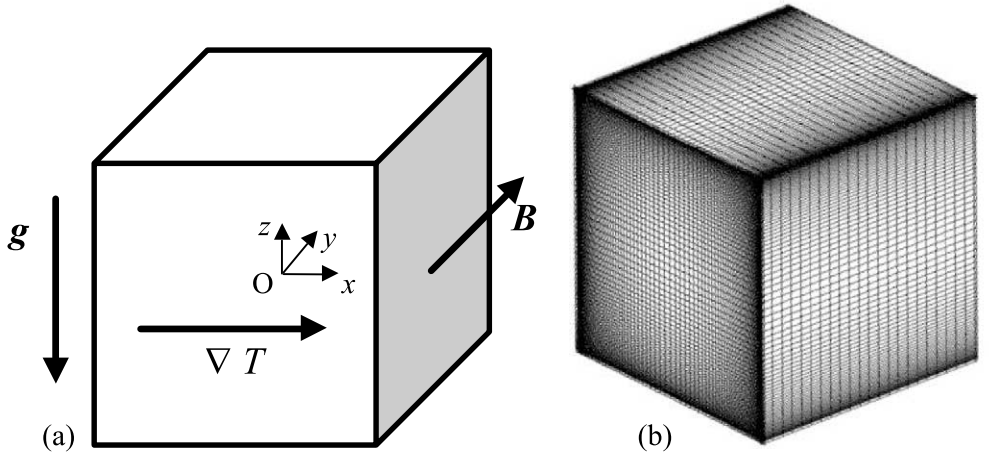

Fig. 1. (a) Sketch of the three-dimensional cubic enclosure; (b) computational grid.

evaluated on the basis of physical coherence and comparison with the few other three-dimensional studies presented in the literature.

2. Model and computational methods

With reference to Fig. 1(a), the Rayleigh number can be defined as

$$Ra = g\beta\Delta\vartheta D^3/(v\alpha) \tag{1}$$

in which β, v and α are the fluid's thermal expansion coefficient, kinematic viscosity, and thermal diffusivity, respectively. The Hartmann number is defined as

$$M = DB(\sigma/\mu)^{1/2} \tag{2}$$

in which σ, ρ and $\mu = \rho v$ are the fluid's electrical conductivity, density, and viscosity, respectively. It can be shown that M^2 represents the ratio of electromagnetic to viscous forces.

The walls normal to the magnetic field are called *Hartmann walls*. In the associated boundary layers, the velocity profile is basically determined by a balance between Lorentz and viscous forces, and their thickness δ_H scales as M^{-1}. The walls parallel to the magnetic field are called *side walls*, and the associated boundary layers, side layers; their thickness δ_S scales as $M^{-1/2}$ [3].

Under the assumption of a low magnetic Reynolds number $Re_m = u_0 D\sigma\eta$ – in which $u_0 = (\alpha/D)(Ra/M^2)$ is a characteristic velocity and η is the fluid's magnetic permeability – the induced magnetic field is negligible with respect to the applied field **B**. Such an inductionless flow is governed by the Navier–Stokes equations with the Lorentz force $\mathbf{J}\times\mathbf{B}$ added to the right-hand side. By using the Boussinesq approximation for buoyancy, assuming steady-state conditions and making all terms dimensionless (see below), these equations become

$$\frac{Gr}{M^4}(\mathbf{v}\cdot\nabla)\mathbf{v} = -\nabla p + \frac{1}{M^2}\nabla^2\mathbf{v} + \mathbf{j}\times\hat{\mathbf{y}} + T\hat{\mathbf{z}} \tag{3}$$

and are complemented by the continuity equation

$$\nabla\cdot\mathbf{v} = 0. \tag{4}$$

The velocity vector $\mathbf{v} = (u, v, w)$ and the current density $\mathbf{j}$ are scaled, respectively, by u_0 and by $j_0 = \sigma u_0 B$. The dimensionless pressure p is the difference between the local and the hydrostatic pressure, scaled by Dj_0B. The dimensionless temperature T is the difference between the local temperature ϑ and the mean temperature $\langle\vartheta\rangle$, divided by the wall-to-wall temperature difference $\Delta\vartheta$.

The current density is given by Ohm's law

$$\mathbf{j} = -\nabla\varphi + \mathbf{v}\times\hat{\mathbf{y}} \tag{5}$$

together with the conservation of the electric charge

$$\nabla\cdot\mathbf{j} = 0. \tag{6}$$

The electrical potential φ is scaled by Du_0B. From Eqs. (5) and (6) a Poisson equation for φ is easily derived

$$\nabla^2\varphi = (\nabla\times\mathbf{v})\hat{\mathbf{y}}. \tag{7}$$

The temperature distribution is governed by the enthalpy transport equation

$$Ra(\mathbf{v}\cdot\nabla)T = \nabla^2 T. \tag{8}$$

The boundary conditions for velocity are the usual no-slip conditions at the walls (see below, however, for the treatment of walls orthogonal to the magnetic field), while the thermal boundary conditions are

$$T = \pm 0.5 \quad \text{at } x = \pm 0.5. \tag{9}$$

Of course, the purely conductive solution is simply $T = x$.

The electrical boundary condition are simply those expressing continuity of electrical potential φ and electrical current $\mathbf{j} = -\sigma\nabla\varphi$ at the fluid–wall interface, with $\mathbf{j} = 0$ on the outer surface of the solid walls. In the present case of plane walls, by integrating across the wall thickness t_w the above conditions can be reconducted to the thin wall condition [4] expressing the conservation of electric charge in the plane of the wall

$$\mathbf{j}\cdot\mathbf{n} = c_w\nabla_w^2\langle\varphi\rangle \tag{10}$$

in which $\langle\varphi\rangle$ is the mean value of φ across the wall, $\mathbf{n}$ is the inward-directed unit vector normal to the wall, and ∇_w^2 is the two-dimensional Laplacian operator in the plane of the wall. The constant c_w is the *wall conductance ratio*, $(\sigma_w t_w)/(\sigma D)$.

The governing Eqs. (3), (4), (7) and (8), with the boundary conditions discussed above, were solved by a finite volume technique using the SIMPLEC pressure–velocity coupling algorithm [5] and the QUICK third-order discretization scheme for the advection terms. The CFD package CFX-4 [6] was used for the simulations, but some adaptations were required since CFX-4 does not explicitly provide for MHD problems [7]. In particular, the electrical potential equation was solved by using the elliptic solvers normally adopted by CFX-4 for the solution of scalar transport equations, appropriately modified so as not to include convection terms. This allowed the problem to be treated as a fully implicit fluid dynamics-scalar transport problem, with no explicit "outer" coupling between hydrodynamic and electrical quantities.

The explicit resolution of the Hartmann layer can be omitted by integrating analytically all equations across it [8,9]. The physical model behind this substitution is that the wall and the layer are considered as electrical resistances connected in parallel. As a result, the wall conductance ratio c_w at the Hartmann wall must be replaced by $c_w + \delta_H$, where $\delta_H = M^{-1}$ is the total conductance of the fluid layer. At the same time, at the

Hartmann walls the first grid point in the fluid must lie outside of the Hartmann layer, and the no-slip condition must be replaced either by a shear-free condition or by a free slip condition (linear extrapolation of the velocity at the wall from the inner grid points). The two conditions are similar and yield practically identical flow fields [10]; the second alternative was adopted here.

The model described above could easily be extended to more complex geometries, including the case of solid walls arbitrarily oriented with respect to the magnetic field. However, in this case the *local* wall conductance ratio should be written as $c_w + (M\mathbf{n}\cdot\hat{\mathbf{y}})^{-1}$, according to the local thickness of the Hartmann layer along the wall surface [11]. As an alternative, a direct simulation of the Hartmann layers could be performed using a fine near-wall grid, with no "synthetic" modelling.

In the present computations, 1500 iterations at most were needed for a complete convergence of all variables; this convergence speed was thus higher than for the quasi-two-dimensional, fully developed, problem [2] and was only slightly affected by the conductivity of the walls, the Grashof number, or the Hartmann number. A grid of $n_x \times n_y \times n_z = 90 \times 24 \times 90 = 194400$ nodes was used for all the simulations, with a non-equispaced distribution in the directions x and z, orthogonal to the magnetic field; it is shown in Fig. 1(b). The magnetic field direction was resolved by a comparatively small number of points since the integral model discussed above was adopted for the Hartmann layer. Some purely hydrodynamic simulations were also performed; for these cases a non-equispaced grid of $n_x \times n_y \times n_z = 60 \times 60 \times 60 = 216000$ nodes was used. All simulations were run on a Pentium III-500 MHz computer with 256 MB RAM and typically required ~40 h of CPU time for each test case.

3. Base flow in the absence of MHD interactions

The three-dimensional flow occurring in the differentially heated cubic enclosure in the *absence* of MHD effects will be considered first, in order to provide a basis for the following discussion.

Davis [12] was among the first to discuss three-dimensional effects for the free convection flow in a differentially heated enclosure. He argued that the interaction of the main circulation roll with the side walls should give rise to a secondary flow with a velocity component parallel to the roll axis. Mallinson et al. [13] presented three-dimensional finite-difference numerical simulations for different aspect ratios, Prandtl numbers ranging from 0.2 to 100 and Rayleigh numbers ranging from 10^4 to 10^5. For an enclosure of aspect ratios 1:2:1 (x:y:z, with the same axis nomenclature as in Fig. 1), they predicted characteristic toroidal circulation cells with the flow moving inward, i.e., toward the mid-plane $y = 0$, in the centre and outward, i.e., toward the side walls, at the periphery. A similar three-dimensional flow pattern was experimentally confirmed by the flow visualization studies of Hiller et al. [14], based on thermochromic liquid crystals suspended in water–glycerol mixtures filling a cubic enclosure ($Pr = 5.8$–6000, $Ra = 10^4$–2×10^7).

More recently, three-dimensional numerical simulations were presented by Janssen et al. [15] for $Pr = 0.71$ (gases) and Ra ranging from 10^5 to 10^8. The authors found only a moderate three-dimensionality, with the flow in the mid-plane $y = 0$ very close to that predicted by two-dimensional simulations. Also the instability mechanisms leading from steady-state to time-periodic and chaotic flow, and the corresponding dominating frequencies, were found to be similar to those predicted by two-dimensional studies; in particular, transition to periodic flow was predicted for $Ra = 2.3 \times 10^6$, only ~10% higher than for a two-dimensional enclosure.

As regards low-Prandtl number fluids (liquid metals), coarse-mesh three-dimensional finite-difference simulations for the free convection of gallium ($Pr = 0.027$) in rectangular enclosures with different aspect ratios were presented by Viskanta et al. [16] and were compared with experimental temperature distributions. The Rayleigh number was $\sim 10^6$; at this Ra, the flow was found to be steady and laminar. The authors observed that three-dimensional effects were significant and, due to the low value of the Prandtl number, extended down to the mid-plane of the cavity instead of being confined to the front and back walls. A correct modelling of the thermal boundary conditions was found to be crucial.

Tagawa and Ozoe [17] conducted numerical simulations for the free convection flow in differentially heated enclosures at $Pr = 0.025$, with and without an external magnetic field perpendicular to the isothermal walls. The configuration was the same discussed here, with two isothermal walls and four adiabatic walls. The authors used a finite-difference, staggered-grid method, the HSMAC pressure–velocity coupling algorithm, and the Utopia third-order differencing scheme for the convective terms. In the absence of a magnetic field, both at $Ra = 10^5$ and 10^6 the flow had not attained a steady-state, but still exhibited significant oscillations, after a simulation time of $\sim 2000 \times Ra^{-2/3} D/\alpha$. However, the finest computational grid used was still rather coarse (46^3 nodes) and the simulations were rather limited in time, so that it is difficult to draw precise conclusions regarding the nature of the oscillations and the influence of numerical factors. Experimental results by the same authors [18], conducted in a differentially heated cubic enclosure filled with liquid gallium at Rayleigh numbers ranging from 1.85×10^6 to 4.75×10^6, also exhibited oscillations in the temperatures measured by thermocouples. The oscillations were apparently random, with no recognizable periodicity.

As regards the present simulations, conducted for a Rayleigh number of 10^5, results are summarized in Figs. 2–4.

Fig. 2 reports in-plane velocity vector plots in the three co-ordinate planes $y = 0$ (a), $z = 0$ (b) and $x = 0$ (c) containing the centre of the cubic enclosure. The (dimensionless) unit velocity vector is reported above each graph; note that a different scale is used for the main circulation in the xz-plane (a) and for the secondary flows occurring in the xy- and yz-planes (b,c).

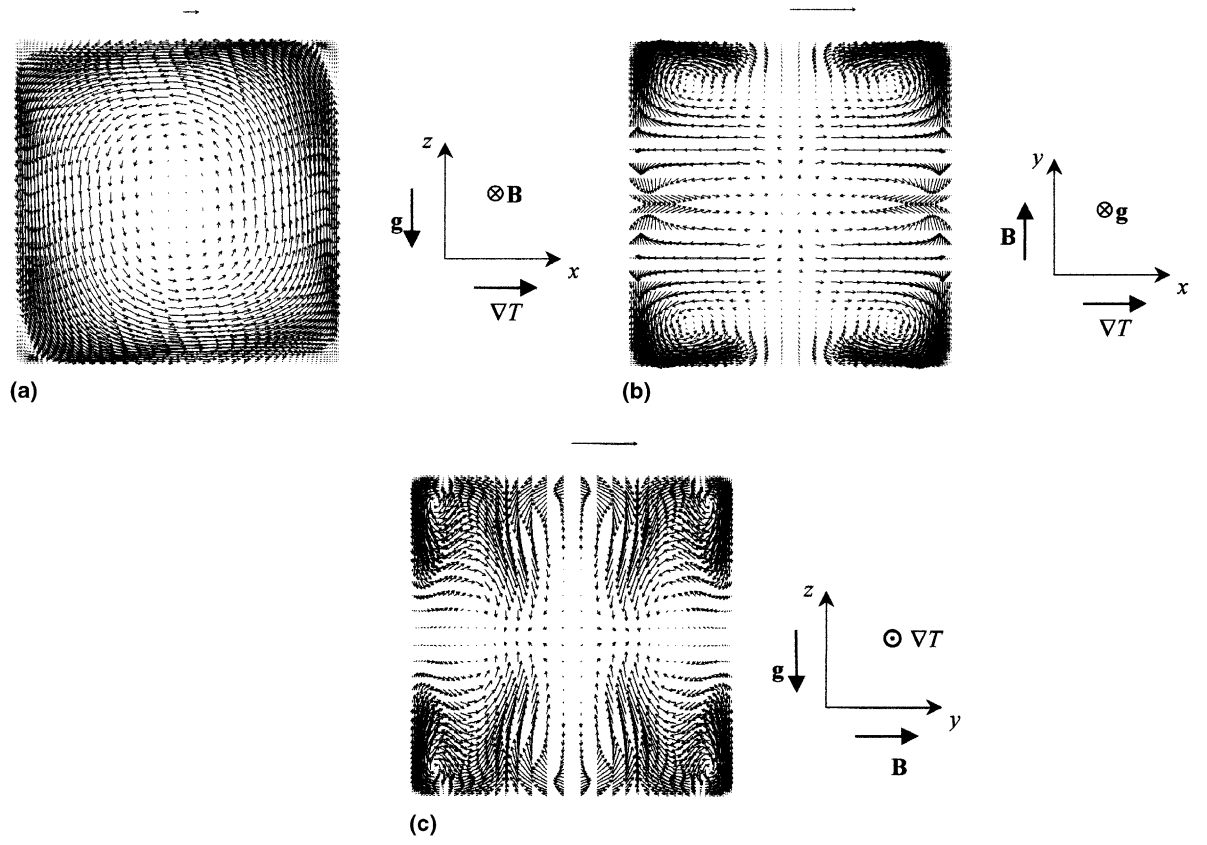

Fig. 2. In-plane velocity vector plots in three orthogonal planes passing by the centre of the enclosure for $Ra = 10^5$ and no MHD: (a) plane $y = 0$; (b) plane $z = 0$; (c) plane $x = 0$. The unit (dimensionless) vector is shown close to each plot. Scaling is based on $M = 100$.

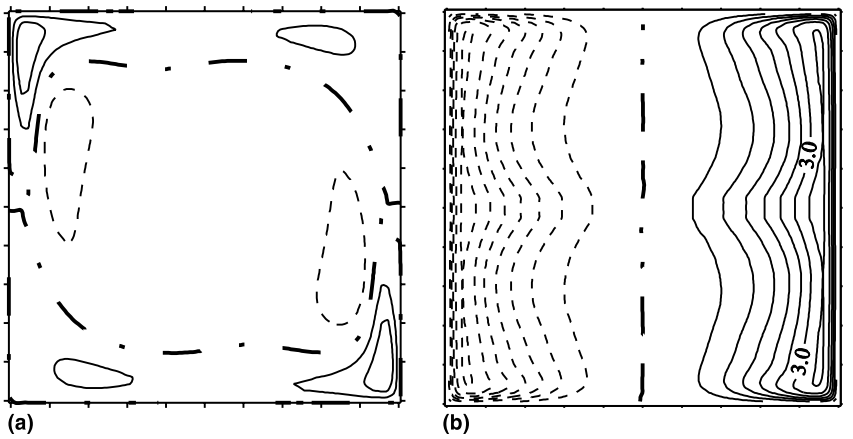

Fig. 3. Secondary flow for $Ra = 10^5$, no MHD. Solid line: negative velocity; broken line: positive velocity; thick line: zero. Scaling is based on $M = 100$: (a) contours of the v component parallel to y in the plane $y = -0.2$; (b) contours of the w component parallel to z in the plane $z = 0$.

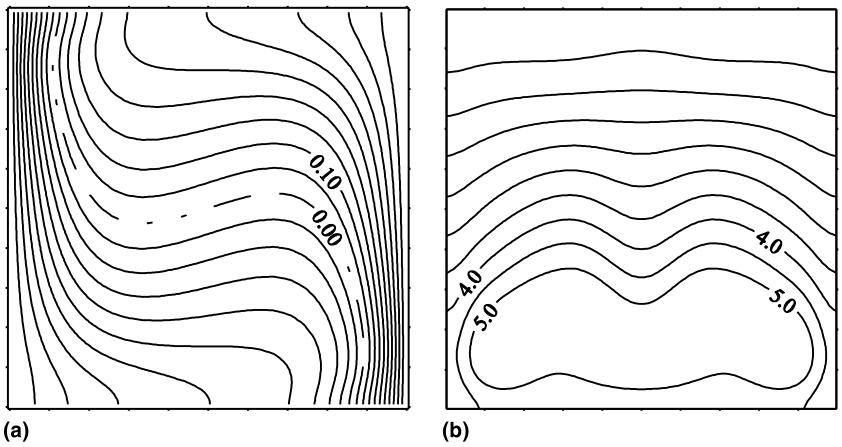

Fig. 4. Heat transfer for $Ra = 10^5$, no MHD. Scaling is based on $M = 100$: (a) temperature in the plane $y = 0$; (b) Nusselt number distribution on the hot (right) wall.

Secondary flows are also shown in Fig. 3, which reports contours of the v velocity component in the plane $y = -0.2$ (a) and of the vertical w component in the mid-plane $z = 0$ (b). Graph (a) shows that, in a constant-y plane located about mid-way between the cavity centre and one of the side walls, the v velocity component is directed towards the mid-plane $y = 0$ in the central region and away from it (i.e., towards the side wall $y = -0.5$) in the periopheral region. This is coherent with the above discussed findings [12–14] of a toroidal three-dimensional circulation in the regions adjacent to the side walls $y = \pm 0.5$. However, maximum centripetal v velocities are attained not near the centre of the constant-y cross-sections, but rather at two anti-symmetric locations which are quite close to the cavity corners and to the peaks of the opposite, centrifugal flow. Figs. 2(b) and (c) confirm that secondary flows mainly consist of complex vortices which do not extend down to the centre of the enclosure but remain more or less confined to the corner regions. The characteristic distortion of the constant-w contours in Fig. 3(b) is a consequence of these secondary flows and indicates that the intensity of the main circulation does not decrease monotonically from the mid-plane $y = 0$ to the side walls, but rather exhibits two symmetrical minima at $y \approx \pm 0.25$.

The temperature distribution in the mid-plane $y = 0$ is reported in Fig. 4(a). Like the flow field, also the isotherm pattern is almost identical to that obtained from two-dimensional simulations for a corresponding square enclosure; it exhibits two thick wall boundary layers and a stably stratified core region, with a weak inverse horizontal T gradient in the central portion of the cavity. The distribution of the Nusselt number (dimensionless heat flux) along the hot-wall $x = 0.5$ is reported in Fig. 4(b). Along the vertical direction, Nu attains its highest values ($\sim$5) close to the bottom wall, in correspondance with the initial development of the hot-wall boundary layer, and decreases for larger y as the boundary layer thickens. Along the horizontal direction, contours of Nu exhibit a characteristic distortion, strictly related to the shape of the vertical velocity contours in Fig. 3(b), which causes absolute maxima of Nu to be attained not on the mid-line $y = 0$, but rather at two off-centre points symmetrically located with respect to it. All the results shown are in close agreement with those obtained by Tagawa and Ozoe [17] for the same Rayleigh number and a very similar Prandtl number.

4. MHD free convection flow

4.1. Review of the literature

A review of buoyant convective magnetohydrodynamic flows was given by Blums et al. [19]. Bühler [20] developed an asymptotic analysis of fully developed flow in a vertical rectangular duct. Such flow is governed by the inertialess equations, and the analysis is valid for well conducting side walls and high Hartmann numbers. Both the differentially heated and the internally heated cases were considered, and the magnetic field was supposed to be parallel to a pair of walls and orthogonal to the others. The results were used to validate the numerical methods in the CFX-4 code [2].

Only few results have been presented in the literature for the present configuration, i.e., cubic enclosure with free convection induced by differential heating. Aleksandrova and Molokov [21] presented a purely diffusive solution.

As mentioned before, Tagawa and Ozoe [17] simulated free convection in a differentially heated cube in the presence of a magnetic field perpendicular to the isothermal walls (the same configuration studied in the present work). The problem was characterized by

$Pr = 0.025$, $Ra = 10^5$ and 10^6, and $M = 0$–10^3. All walls were assumed to be electrically non-conducting. Interestingly, under these conditions a weak magnetic field (Hartmann number up to 100–200) was found slightly to *enhance* heat transfer, causing the average Nusselt number to increase by 5–7%, and also to enhance the peak velocity attained near the hot and cold walls. The moderate increase in heat transfer for M up to ~100–200 was also confirmed by the experiments conducted by the same authors in liquid gallium [18] at $Ra = 1.85 \times 10^6$ to 4.75×10^6. Both effects were explained by the electric current pattern established near the edges between the Hartmann walls and the isothermal walls, which combined with the imposed magnetic field so as to *assist* the buoyant flow and to contrast the viscous forces exerted by the walls. Only for $M > 200$ the decelerating effects of the Lorentz forces near the central regions of the hot and cold walls became dominant, and both peak velocities and heat transfer rates decreased with M.

A more complete numerical analysis was conducted by Tagawa and Ozoe [22] for $Ra = 10^5$, $M = 100$, and $Pr = 0.025$, by letting the wall conductance ratio c_w vary from 0 to ∞. The computational grid was rather coarse (32 nodes in each direction, with only 22 points in the fluid itself, and five points in each wall). Thus, the side layers were not properly discretized, and the Hartmann layer was neither modelled nor directly resolved by a sufficiently large number of grid points. This is actually unphysical, especially for the lower values of the wall conductance ratio, when the currents close themselves almost completely through the boundary layers rather than through the solid walls. The results will be considered later and compared with the present predictions.

As regards *experimental* results, the work by Tagawa and Ozoe [18] was mentioned above. Measurements of the effects of a vertical magnetic field on Rayleigh–Bénard convection with the sodium–potassium alloy NaK ($Pr \sim 1.9 \times 10^{-2}$ at 393 K) were presented by Burr et al. [23]. The average Nusselt numbers for $Ra \sim 10^3$–10^5 and a Chandrasekar number $BH^2\sigma/\mu$ up to $\sim 1.4 \times 10^4$ (H being the height of the enclosure) were compared with previous numerical simulations, and the possibility of a time-dependent flow was proved. In a companion report [24] the effect of a horizontal transverse magnetic field was studied in the same range of parameters, and a quasi-two-dimensional model for the core was proposed for buoyant flow; this model is close to the model presented by Bühler [25], but the buoyancy term was added.

Experimental results for the natural convection induced by differential-heating with liquid NaK and a

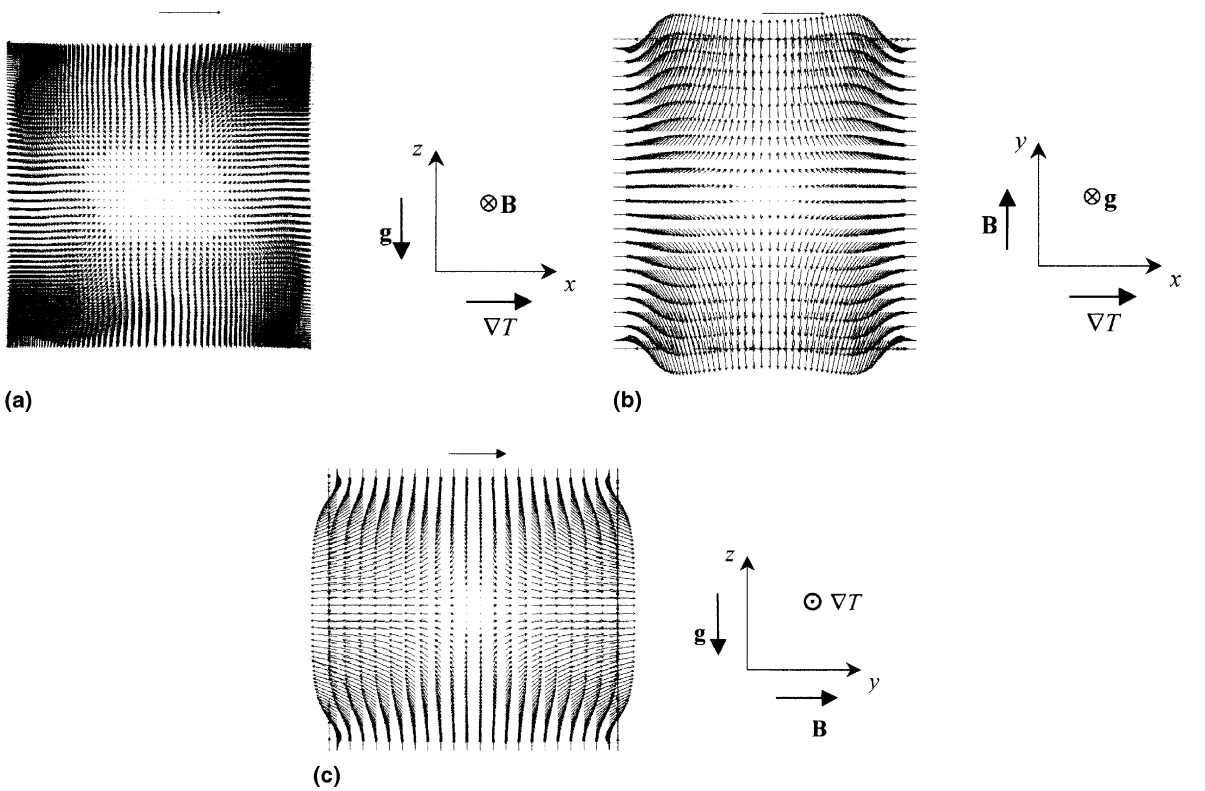

Fig. 5. Electric current density **j** in three orthogonal planes passing by the centre of the enclosure for $Ra = 10^5$, $M = 100$ and perfectly conducting walls: (a) plane $y = 0$; (b) plane $z = 0$; (c) plane $x = 0$. The unit (dimensionless) **j** vector is shown above each plot.

magnetic field orthogonal to the horizontal temperature gradient and to gravity were presented by Fumizawa [26]. The range of parameters investigated was M up to 10^4 and $Ra \sim 10^7$–10^8. The electrical boundary conditions are not clear, especially at the Hartmann walls, and for this reason a full understanding of the results is difficult. The configuration was similar to that assumed in the present work (cubic enclosure), but in the work of Fumizawa the Rayleigh number was higher and the cavity was slender. The consequent larger importance of convection perhaps explains the high Nusselt numbers reported (up to 30).

4.2. The case $M = 100$, $c_w = \infty$ (perfectly conducting walls)

Results will be presented here for a typical MHD test case, characterized by a Hartmann number $M = 100$ and $c_w \to \infty$ (perfectly conducting walls). The pattern of the electric current density vector **j** is shown in Fig. 5. Graphs (a)–(c) refer to the principal planes $y = 0$, $z = 0$ and $x = 0$, respectively. The most relevant component of the current density is that parallel to the magnetic field **B**, as shown in the xy (b) and yz (c) cross-sections, where the **j** vector is seen to enter orthogonally the Hartmann walls. The components of **j** in the plane xz orthogonal to **B** (a) are much smaller.

For the same case, the velocity vector plot in the mid-plane $y = 0$ is reported in Fig. 6(a). The main flow is considerably less intense than the base flow with no MHD, see Fig. 2(a), and exhibits a square-shaped circulation cell in contrast with the circular cell of the base flow. Secondary flows (not reported) are very weak, showing that three-dimensionality is almost completely suppressed by MHD interactions in the cubic enclosure.

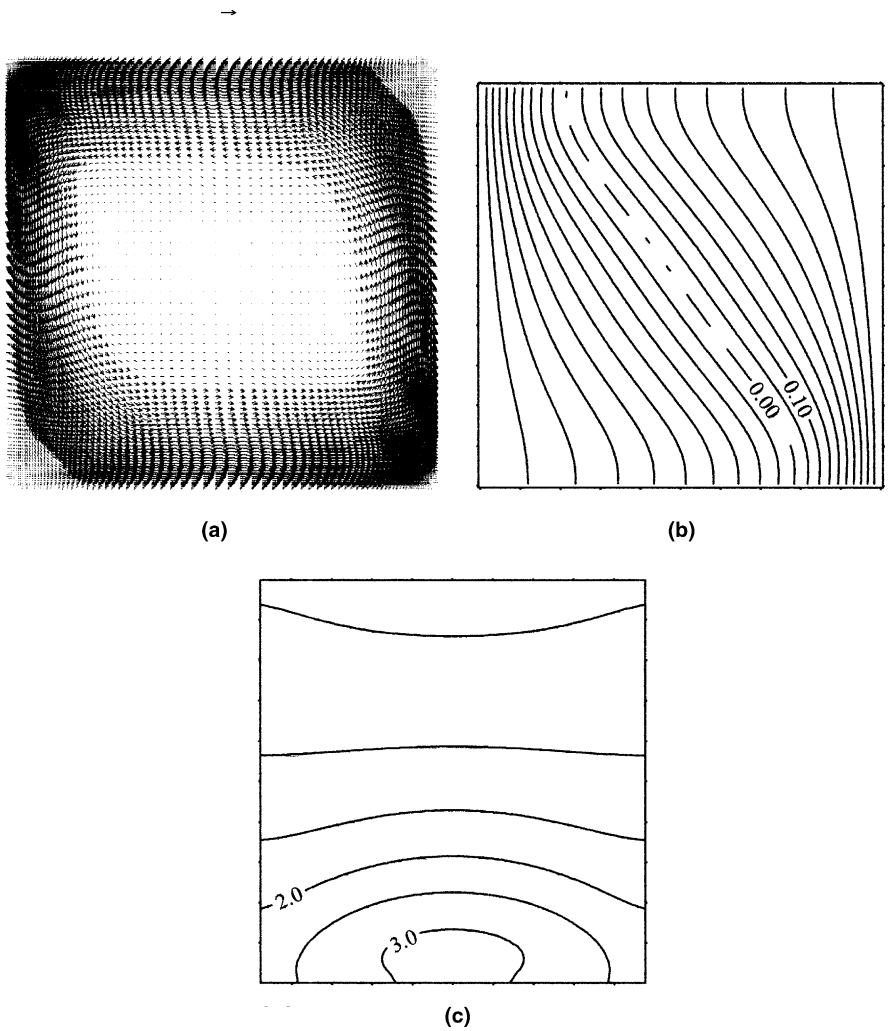

Fig. 6. Results for $Ra = 10^5$, $M = 100$ and perfectly conducting walls: (a) in-plane velocity vector plots in the mid-plane $y = 0$. The unit (dimensionless) velocity vector is shown; (b) temperature in the mid-plane $y = 0$; (c) Nusselt number distribution on the hot (right) wall.

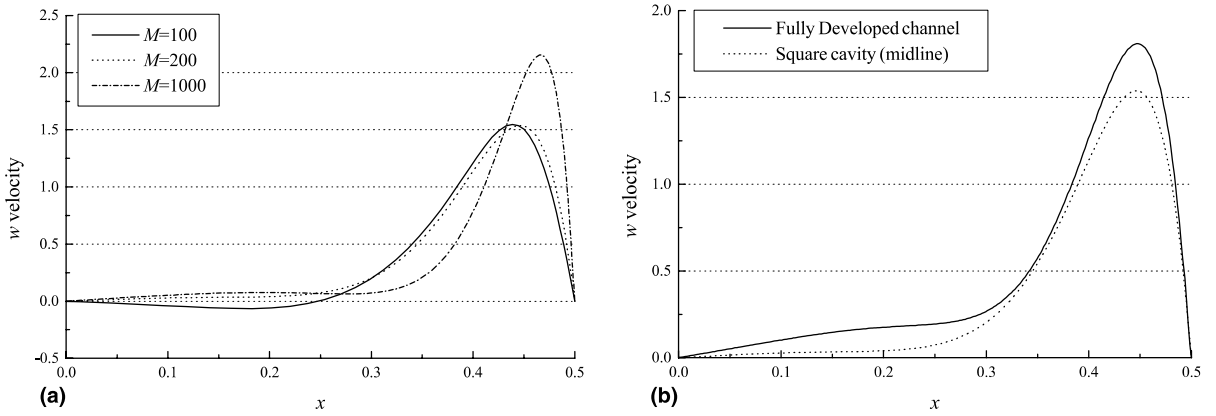

Fig. 7. Velocity profiles along the x axis for $Ra = 10^5$, $c_w \to \infty$: (a) solutions at various Hartmann number; (b) comparison with the fully developed channel solution (2) for $M = 200$.

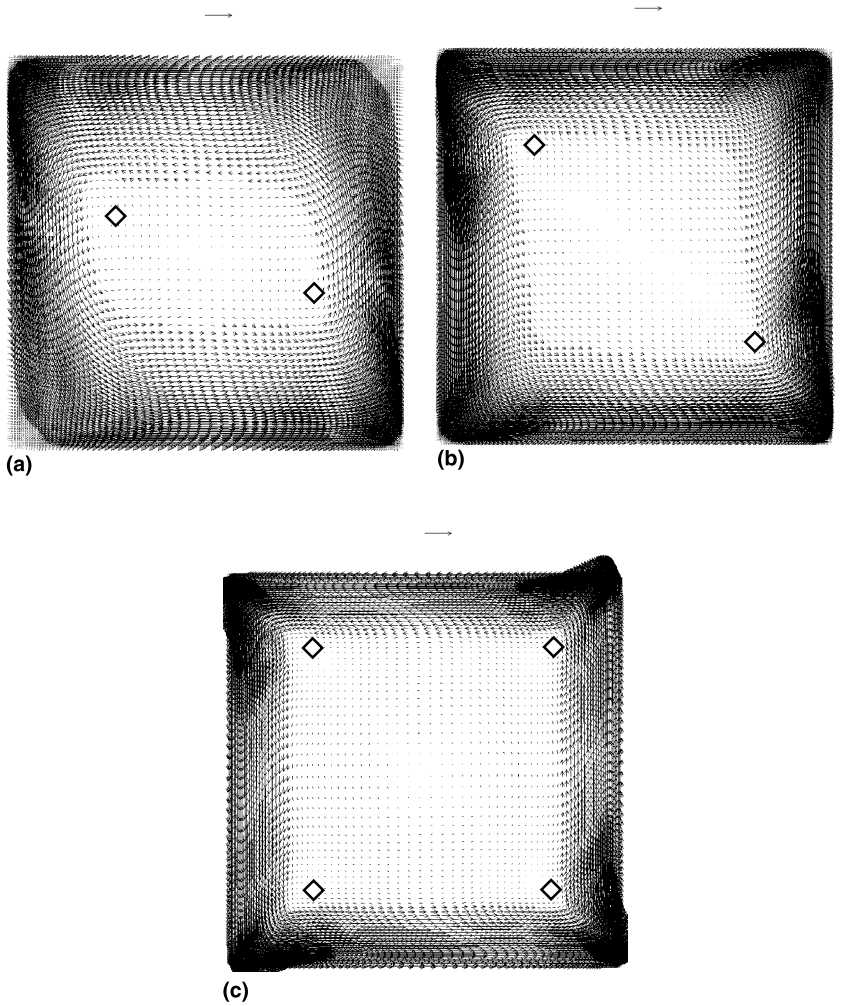

Fig. 8. Velocity vectors in the plane $y = 0$ for $Ra = 10^5$, $c_w \to \infty$. The circulation centres are indicated by small diamonds: (a) $M = 100$; (b) $M = 200$; (c) $M = 1000$.

The temperature distribution in the plane $y = 0$ and the Nusselt number distribution on the hot active wall $x = 0.5$ are reported in Figs. 6(b) and (c) and can be compared with the results obtained for the case of no MHD in Fig. 3. Vertical thermal stratification is largely suppressed by MHD effects, and peak values of the Nusselt number are reduced from ~5 to ~3. Also the characteristic shape of the constant-*Nu* lines in Fig. 3(b), associated with the spanwise variation of the vertical velocity in the base flow, is absent in the MHD case.

4.3. Influence of the Hartmann number

The effect of the Hartmann number M was investigated by repeating the simulations for $Ra = 10^5$, perfectly conducting walls ($c_w \to \infty$) and three values of M (100, 200, and 1000).

The velocity profiles obtained along the x axis are shown in Fig. 7(a). The solutions for $M = 100$ and 200 are similar in the side boundary layer, while in the core the positive slope of the profile is recovered for $M = 200$. A comparison of velocity profiles in the mid-line for the fully developed channel flow [2] and the present cubical enclosure for $M = 200$, Fig. 7(b), shows that in the side layers the velocity peak is of the same order (~1.55 against ~1.77), while the flow rate carried in the core region is much higher in the fully developed case.

Fig. 8 shows the velocity vector plots in the plane $y = 0$; the thickness of the side layers decreases for $M = 1000$, as can be seen also in Fig. 7(a). The shape of the circulation cells becomes increasingly square for increasing Hartmann numbers, and two circulation centres (conventionally indicated by small diamonds) are present. In the case $M = 100$ the circulation centre on the right side is located just below mid-height, and that on the left side just above; circulation centres move towards the corners as M increases, and thus do not affect the velocity profiles in the mid-line $z = 0$ for the higher values of the Hartmann number ($M = 200, 1000$). For $M = 1000$, Fig. 8(c), two more circulation centres appear in the top-right and left-bottom corners, and a weak circular cell is present in the core of the cavity.

An interesting correspondence exists between the velocity vector plots and the electrical potential distri-

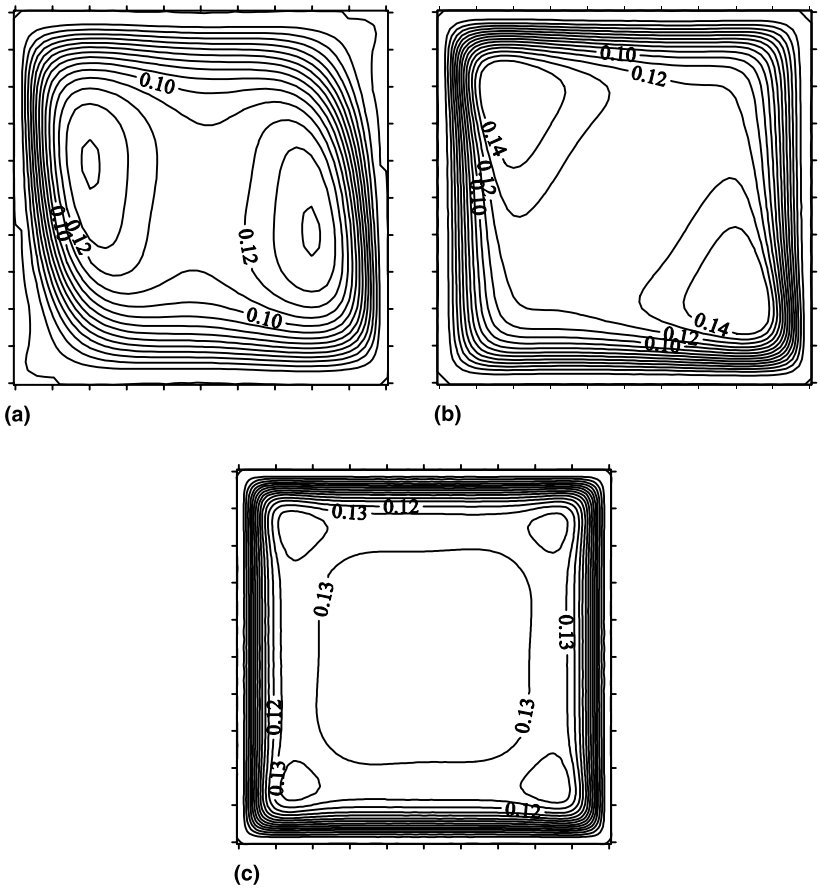

Fig. 9. Electrical potential contours in the plane $y = 0$ for $Ra = 10^5$, $c_w \to \infty$: (a) $M = 100$; (b) $M = 200$; (c) $M = 1000$.

bution in the same plane $y = 0$, reported in Fig. 9; in particular, it can be observed that the centres of the circulation cells tend to coincide with the relative maxima of the electrical potential φ. This can be explained by considering that, neglecting the curvature of potential in the magnetic field direction, the Laplacian of φ in the plane $y = 0$ gives the component of vorticity in the direction of the magnetic field; this vorticity is responsible for the circulation shown in Fig. 8. The distribution of the electrical potential in the plane $y = 0$ is strongly influenced by the top and bottom walls, and thus also inverse velocity profiles in the core of the domain are possible.

The temperature distribution in the same plane $y = 0$, Fig. 10, tends to the purely conductive solution (horizontal stratification only) as the Hartmann number increases; as a result, the average Nusselt number Nu decreases from 1.403 ($M = 100$) to 1.045 ($M = 200$) and 1.007 ($M = 1000$). The flow rate carried by the circulation cell, once normalized by $u_0 D$, changes little with M, ranging from $\sim$0.135 for $M = 100$ to $\sim$0.150 for $M = 1000$.

4.4. Influence of the wall conductance ratio

Fig. 11 reports vector plots of the current density vector **j** in the horizontal mid-plane $z = 0$ for different values of the wall conductance ratio c_w. A perfect symmetry can be observed in both the x and y directions. The currents in the plane $x = 0$ (not reported) are of the same order of magnitude as in the plane $z = 0$ and have a similar interpretation, since for this plane the top and bottom boundary layers play the role of *side layers*, while the currents in the plane $y = 0$ are much lower. For the lower wall conductance high current jets flow parallel to the side walls, graphs (a)–(c). The z-component of such current damps the flow boundary layer close to the top and bottom walls. The current patterns obtained for $c_w = 1$ are already practically identical to those computed for $c_w \to \infty$, see Fig. 5(b).

Fig. 12 reports the velocity vector plots in the mid-plane $y = 0$ as c_w increases from 0 (insulating walls) to 1. Note that the base flow obtained for no magnetohydrodynamic interactions, normalized by the magnetic

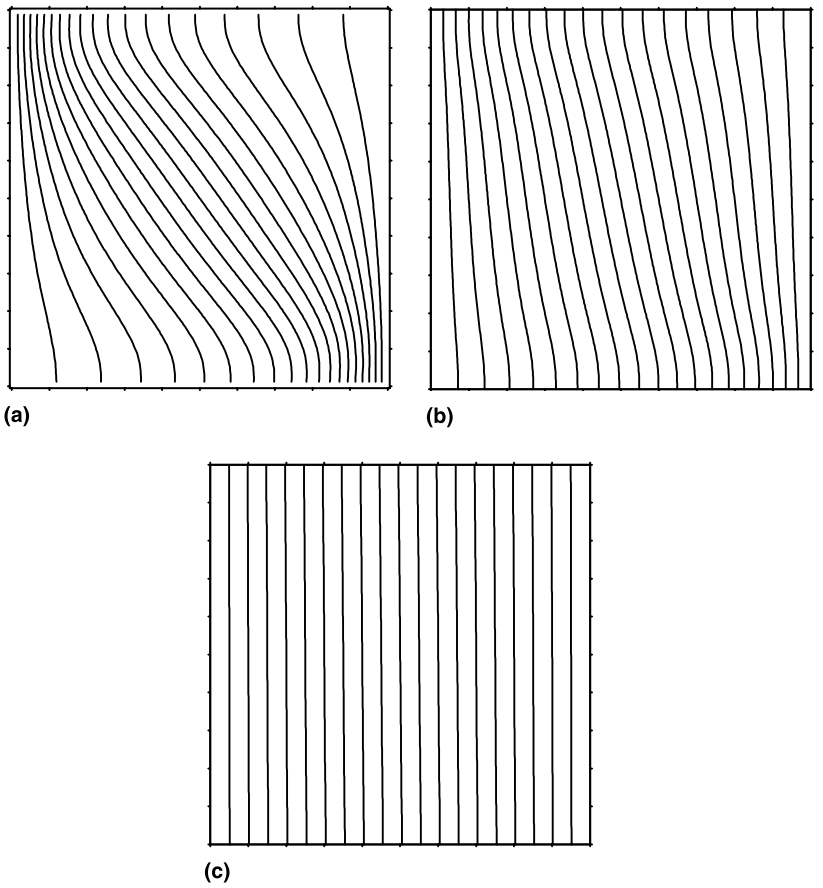

Fig. 10. Temperature contours in the mid-plane $y = 0$ for $Ra = 10^5$, $c_w \to \infty$: (a) $M = 100$; (b) $M = 200$; (c) $M = 1000$.

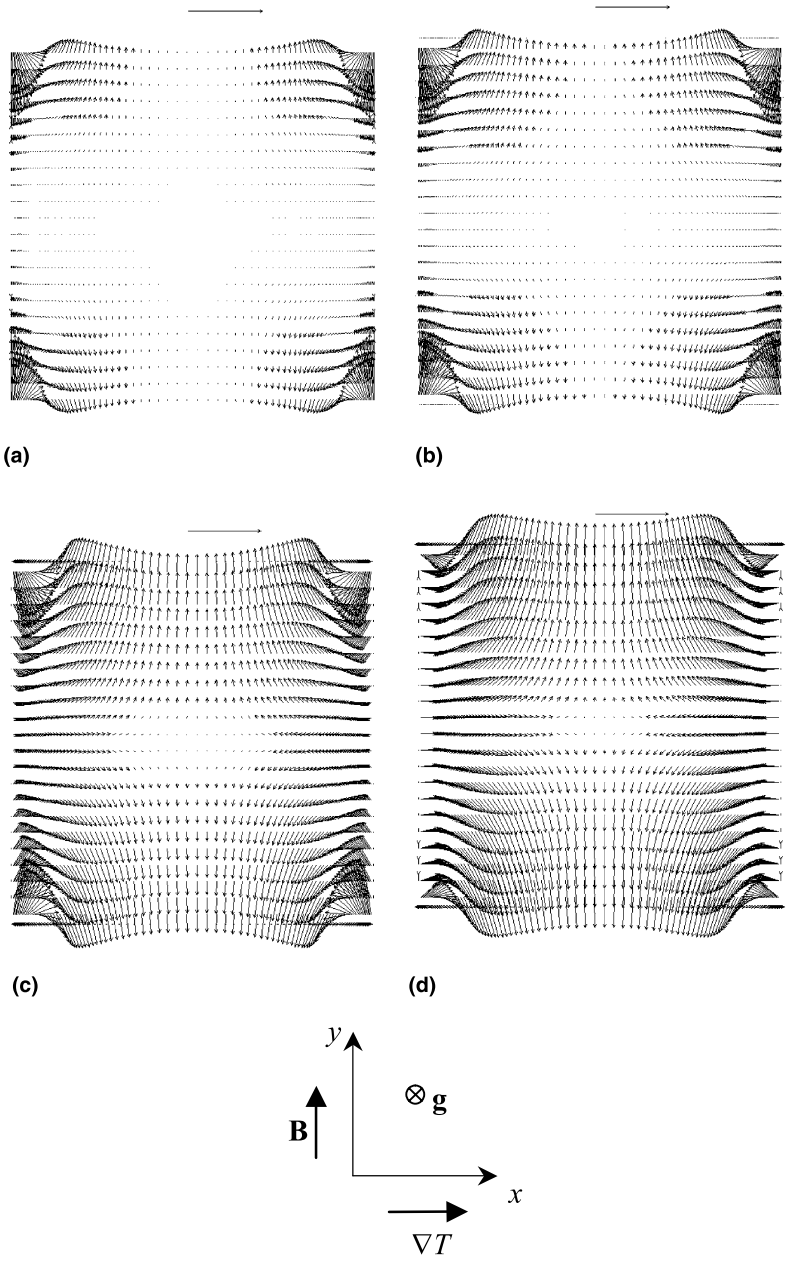

Fig. 11. Total current density **j** in the horizontal mid-plane $z = 0$ for $M = 100$, $Ra = 10^5$. The unit (dimensionless) **j** vector is shown above each plot: (a) $c_w = 0$; (b) $c_w = 0.01$; (c) $c_w = 0.1$; (d) $c_w = 1$.

scale corresponding to $M = 100$, was reported in Fig. 2(a), and the solution for $c_w \to \infty$ (infinitely conducting walls) in Fig. 6(a). The base flow exhibits a circulation cell that is basically circular in shape, with small shear-induced counter-rotating cells in the top-right and bottom-left corners. The main effects of the magnetic field are to change the shape of the cell from circular to square, to modify the thickness of the wall boundary layers and to suppress the counter rotating cells at the corners. The currents, and thus the Lorentz forces are stronger for the higher values of c_w, giving rise to a weaker convective transport. The solution for $c_w = 1$ is practically coincident with that obtained for $c_w \to \infty$.

The influence of c_w is better evidenced from a quantitative point of view by the line graphs in Fig. 13, where the vertical velocity w and temperature profiles along the x-axis are reported. The vertical velocity

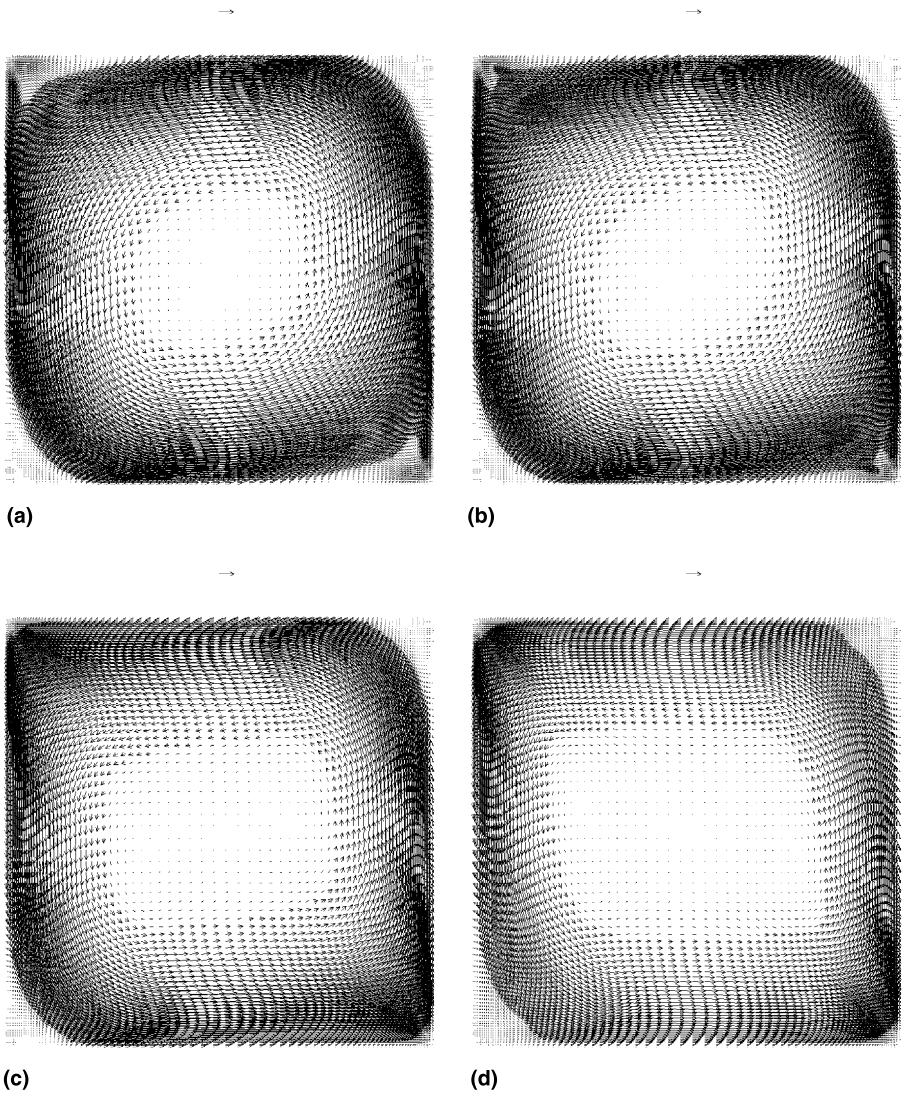

Fig. 12. Velocity vectors in the mid-plane $y = 0$ for $M = 100$, $Ra = 10^5$. The unit (dimensionless) vector is shown above each plot: (a) $c_w = 0$; (b) $c_w = 0.01$; (c) $c_w = 0.1$; (d) $c_w = 1$.

profiles are qualitatively different from those obtained in the fully developed case (2); in particular, convection is almost suppressed in the core region, and the linear profile which can be obtained from a simple two-dimensional balance of Lorentz and buoyancy forces is not present for any value of c_w. A weak reverse flow (against buoyancy) is obtained for well conducting walls ($c_w = 1$ and $c_w \to \infty$), resulting in the reverse slope of the w profiles for $|x| < 0.3$ in Fig. 13(a). This behaviour can be explained by the presence of the top and bottom walls and by the three-dimensionality of the flow.

Fig. 14 presents the temperature distributions in the plane $y = 0$ (mid-plane orthogonal to the magnetic field) as c_w increases from 0 to 1. The base solution with no MHD interactions and the solution for $c_w \to \infty$ were reported in Figs. 4(a) and 6(b), respectively. For increasing wall conductance ratio, the increasing damping of convection due to the higher currents is evidenced by the progressive dominance of horizontal thermal stratification.

Table 1 shows a comparison between the present predictions for the average Nusselt number, defined as $Nu = (q''D)/(\lambda\Delta\vartheta) = \partial T/\partial x|_w$, and the results obtained by Tagawa and Ozoe [22] for different values of the wall conductance ratio c_w. The best agreement is obtained for the higher values of c_w, when the electrical properties of the walls actually control the current pattern and thus

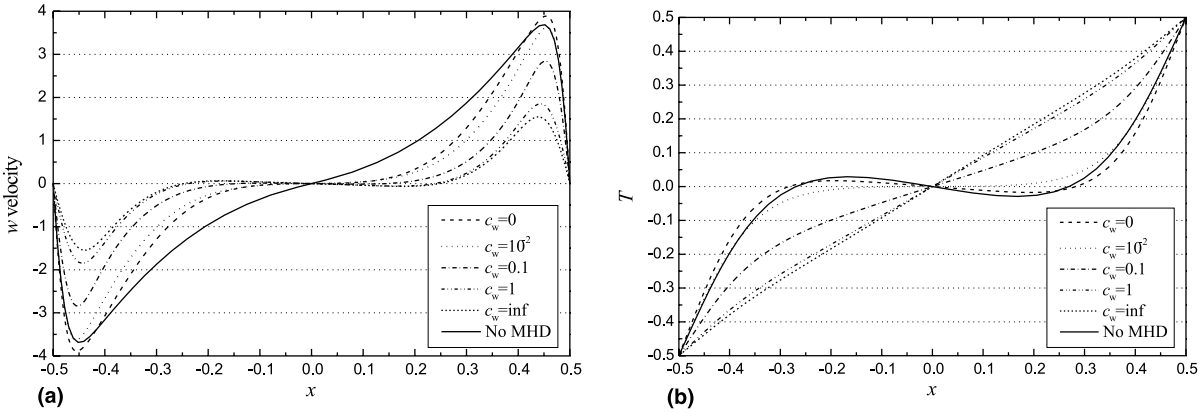

Fig. 13. Velocity (a) and temperature (b) profiles along the x axis for $M = 100$, $Ra = 10^5$ and different values of c_w.

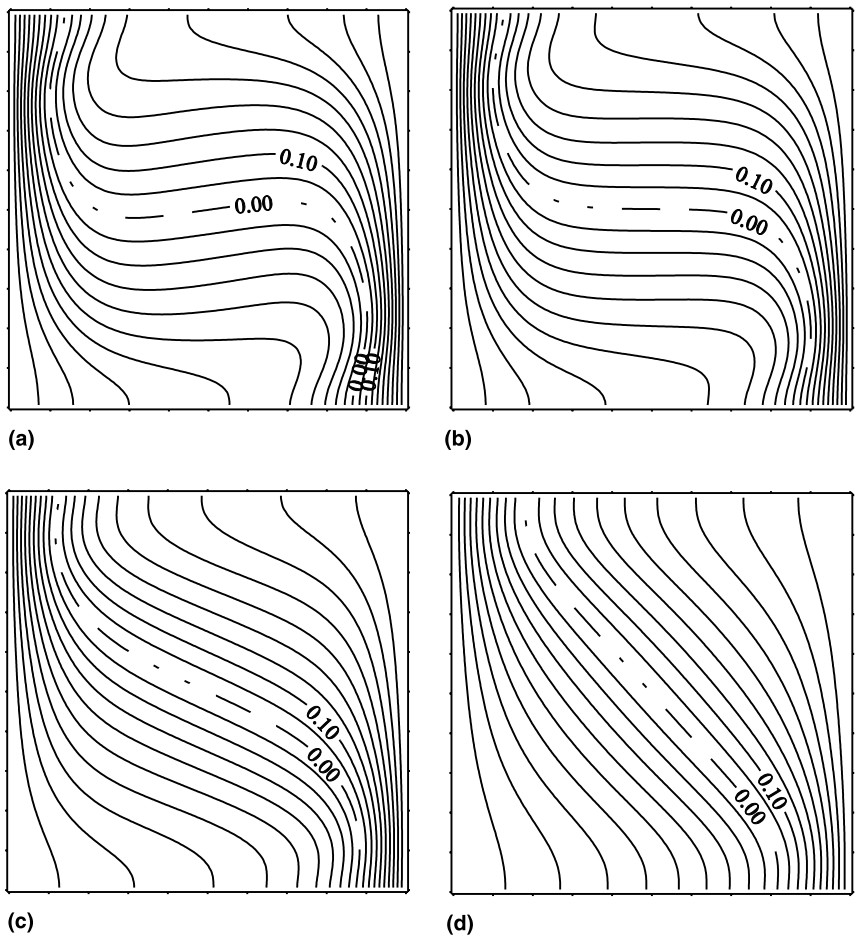

Fig. 14. Temperature in the mid-plane $y = 0$ for $M = 100$, $Ra = 10^5$: (a) $c_w = 0$; (b) $c_w = 0.01$; (c) $c_w = 0.1$; (d) $c_w = 1$.

the discretization of the boundary layers becomes less important, while a discrepancy of ~20% is observed for $c_w = 0$ (insulating walls).

Table 2 reports the average friction coefficient (shear stress made dimensionless by ρu_0^2), the flow rate carried by the main circulation cell, normalized by $\rho u_0 D^2$, and

Table 1
Influence of the wall conductance ratio c_w on the average Nusselt number for a differentially heated enclosure, with $Ra = 10^5$, $M = 100$

c_w	Present study	Tagawa and Ozoe [22]
0	3.286	2.728
0.01	3.092	2.646
0.1	2.334	2.180
1	1.567	1.540
∞	1.403	1.363
No MHD	3.267	2.789

Table 2
Influence of the wall conductance ratio on some overall parameters

c_w	Nu	Flow rate (dimensionless)	$\langle C_f \rangle$
∞	1.403	0.135	0.110
1	1.567	0.168	0.135
0.1	2.334	0.311	0.237
0.01	3.092	0.504	0.302
0	3.286	0.588	0.309
No MHD	3.267	0.615	0.338

the average Nusselt number for the cases simulated. It can be observed that the dimensionless flow rate increases when c_w decreases, ranging from $\sim$0.13 ($c_w \to \infty$) to $\sim$0.58 ($c_w = 0$), and is highest for the case in which MHD is absent (flow rate $\sim$0.61). The friction coefficient exhibits the same monotonic behaviour, ranging from $\sim$0.11 ($c_w \to \infty$) to $\sim$0.31 ($c_w = 0$), and being $\sim$0.34 without MHD. The Nusselt number attains a slightly higher value ($\sim$3.29) for MHD active and $c_w = 0$ than for no MHD ($\sim$3.27), but the difference is very small and can probably be reconducted to the different computational grids adopted.

5. Conclusions

Three-dimensional numerical simulations were conducted for the MHD buoyancy-driven flow in a differentially heated cubic enclosure using a suitably modified version of the CFX-4 software. The proper implementation of an MHD problem within this code was discussed, with particular attention to the Lorentz forces, the potential equation and the treatment of electrical quantities. The method adopted in the present study is quite general and allows practical configurations to be dealt with by using body-fitted co-ordinates, with an arbitrary electrical conductivity of the walls; pressure-driven flows can also be simulated and it is possible to study separate, but electrically coupled, flow regions and configurations with insulating coatings.

With respect to the previously studied fully developed flow case, the suppression of the flow field was found to be stronger in the core, and a complex three-dimensional flow (with secondary motions) and current pattern was predicted in the fluid domain. A weak reverse flow (against buoyancy) occurred in the core region, and was associated with the presence of two centres of circulation in the left- and right-hand sides of the enclosure. An analogy was observed between stream function Ψ and electrical potential φ in the mid-plane orthogonal to the magnetic field **B**, due to the fact that the component of vorticity in the magnetic field direction acts as a source term in the electrical potential equation.

The effects of the Hartmann number M and of the wall conductance ratio c_w were investigated. Increasing M (e.g., from 100 to 1000) suppressed convective motions and exalted the square-shape of the circulation cells. Increasing c_w (from perfectly insulating to perfectly conducting walls) progressively suppressed convective transport.

The related case of a cubic enclosure with *internal* heat generation is the subject of a companion paper [27].

References

[1] F. Carré, E. Proust, J. Remolouv, A. Racaboy, Z. Tilliette, Fusion reactor blanket – comparative evaluation study, Rapport EMT/SERMA/BP/84/No. 584 T, 3591-21-000, January 17, 1984.
[2] I. Di Piazza, L. Bühler, A general computational approach for magnetohydrodynamic flows using the CFX code: buoyant flow through a vertical square channel, Fusion Technol. 38 (2) (2000) 180–189.
[3] R. Moreau, Magnetohydrodynamics, Kluwer Academic Publisher, Amsterdam, 1990.
[4] J.S. Walker, Magnetohydrodynamic flows in rectangular ducts with thin conducting walls, J. Méch. 20 (1) (1981) 79–112.
[5] J.R. Van Doormal, G.D. Raithby, Enhancements of the SIMPLE method for predicting incompressible flows, Numer. Heat Transfer 7 (1984) 147–163.
[6] Noauthor, CFX-4.2: Solver, CFX-International, Harwell Laboratories, United Kingdom, 1997.
[7] I. Di Piazza, Prediction of free convection in liquid metals with internal heat generation and/or magnetohydrodynamic interactions, Doctoral Thesis in Nuclear Engineering, University of Palermo, 2000.
[8] L. Leboucher, Numerical simulation of unsteady magnetohydrodynamic flows in ducts, Technical report FZKA 5663, Forschungszentrun Karlsruhe, 1995.
[9] B. Mück, Numerische Untersuchung von Strömumgen in Kanälen mit Versperrungen unter dem Einfluß von Magnetfeldern, Technical report FZKA 6292, Forschungszentrum Karlsruhe, 1998.
[10] L. Leboucher, Monotone scheme and boundary conditions for finite volume simulation of magnetohydrodynamic

internal flows at high Hartmann number, J. Comput. Phys. 150 (1999) 181–198.
[11] L. Bühler, Magnetohydrodynamic flows in arbitrary geometries in strong, nonuniform magnetic fields – a numerical code for the design of fusion reactor blankets, Fusion Technol. 27 (1994) 3–24.
[12] S.H. Davis, J. Fluid Mech. 30 (1967) 465.
[13] G.D. Mallinson, G. de Vahl Davis, Three-dimensional natural convection in a box: a numerical study, J. Fluid Mech. 83 (1977) 1–31.
[14] W.J. Hiller, S. Koch, T.A. Kowalewski, Three-dimensional structures in laminar natural convection in a cube shaped enclosure, in: P.K. Shah, E.N. Ganiç, K.T. Yang (Eds.), Experimental Heat Transfer, Fluid Mechanics, and Thermodynamics, Elsevier, Amsterdam, 1988, pp. 722–729.
[15] R.J.A. Janssen, R.A.W.M. Henkes, C.J. Hoogendoorn, Transition to time-periodicity of a natural-convection flow in a 3D differentially heated cavity, Int. J. Heat Mass Transfer 36 (11) (1993) 2927–2940.
[16] R. Viskanta, D.M. Kim, C. Gau, Three-dimensional natural convection heat transfer of a liquid metal in a cavity, Int. J. Heat Mass Transfer 29 (1986) 475–485.
[17] T. Tagawa, H. Ozoe, Enhancement of heat transfer rate by application of a static magnetic field during natural convection of liquid metal in a cube, ASME J. Heat Transfer 119 (1997) 265–271.
[18] T. Tagawa, H. Ozoe, Enhanced heat transfer rate measured for natural convection in liquid gallium in a cubical enclosure under a static magnetic field, ASME J. Heat Transfer 120 (1998) 1027–1032.
[19] E. Blums, Y. Mikhailov, R. Ozols, Heat and Mass Transfer in MHD Flows, World Scientific, Singapore, 1987.
[20] L. Bühler, Laminar buoyant magnetohydrodynamic flow in vertical rectangular ducts, Phys. Fluids 10 (1) (1998) 223–236.
[21] S. Aleksandrova, S. Molokov, Three-dimensional buoyant convection in a rectangular cavity with differentially heated walls in a strong, uniform magnetic field: vertical field, Technical report No.99/2, School of Mathematics and Information Sciences, University of Warwick and Coventry University, 1999.
[22] T. Tagawa, H. Ozoe, The natural convection of liquid metal in a cubical enclosure with various electro-conductivities of the wall under the magnetic field, Int. J. Heat Mass Transfer 41 (1998) 1917–1928.
[23] U. Burr, L. Barleon, K.J. Mack, U. Müller, The effect of a vertical magnetic field on liquid metal Rayleigh–Bénard convection, Technical report FZKA 6267, Forschungszentrum Karlsruhe, 1999.
[24] U. Burr, L. Barleon, K.J. Mack, U. Müller, The effect of a horizontal magnetic field on liquid metal Rayleigh–Bénard convection, Technical report FZKA 6267, Forschungszentrum Karlsruhe, 1999.
[25] L. Bühler, Instabilities in quasi-two-dimensional magnetohydrodynamic flows, J. Fluid Mech. 326 (1996) 125–150.
[26] M. Fumizawa, Natural convection experiment with liquid NaK under transverse magnetic field, J. Nucl. Sci. Technol. 17 (2) (1980) 98–105.
[27] I. Di Piazza, M. Ciofalo, MHD free convection in a liquid-metal filled cubic enclosure. II. Internal heating, Int. J. Heat and Mass Transfer 45 (7) (2002) 1493–1511.